



10-Year climatology of vertical profiles (QVPs) of BoXPol in stratiform conditions

T. Scharbach^{1,2}, S. Trömel¹

¹ Institute for Geosciences, Department Meteorology, University of Bonn, 53121, Germany;

² toscha@uni-bonn.de



photo of Bonn X-band radar by V. Pejic

Creation of the large climatology → workflow

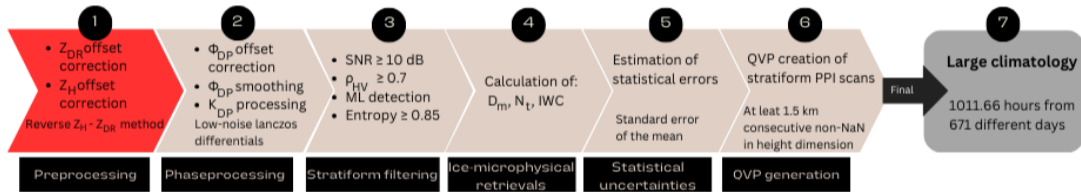


Figure 1: Workflow for creating large climatology of QVPs obtained from BoXPoI data between 2013 and 2023.

Calibration processes + validation using different techniques of Z_H calibration.

Motivation

Precise radar calibration (Z_{DR} and Z_H) is absolutely necessary.

- Strong dependence of methods like e.g. hydrometeor classification, microphysical retrievals or quantitative precipitation estimation (QPE).

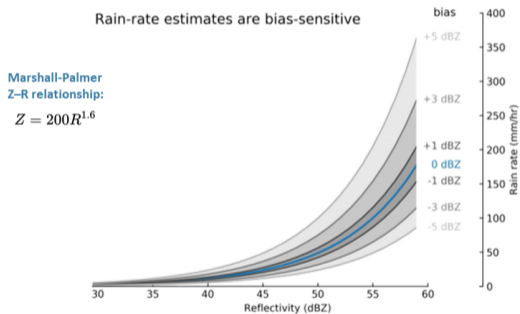


Figure 2: Z_H vs rain rate estimates for different Z_H biases taken from Crisologo, 2019.

Z_{DR} calibration using QVPs in light rain and best fits of Z_H

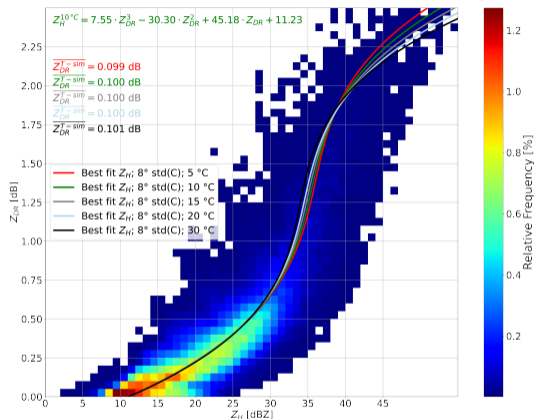


Figure 3: Z_H - Z_{DR} relationship based on T-matrix scattering simulations at 18° elevation angle and 10°C using disdrometer measurements [Chen et al., 2021].

$$Z_{DR}^{off} = med_{day} [mean_{height} (Z_{DR}^{QVP}) - (\overline{Z_{DR}^{T-sim}})]$$

Comparison of Z_{DR} corrected with QVPs and the birdbath scan

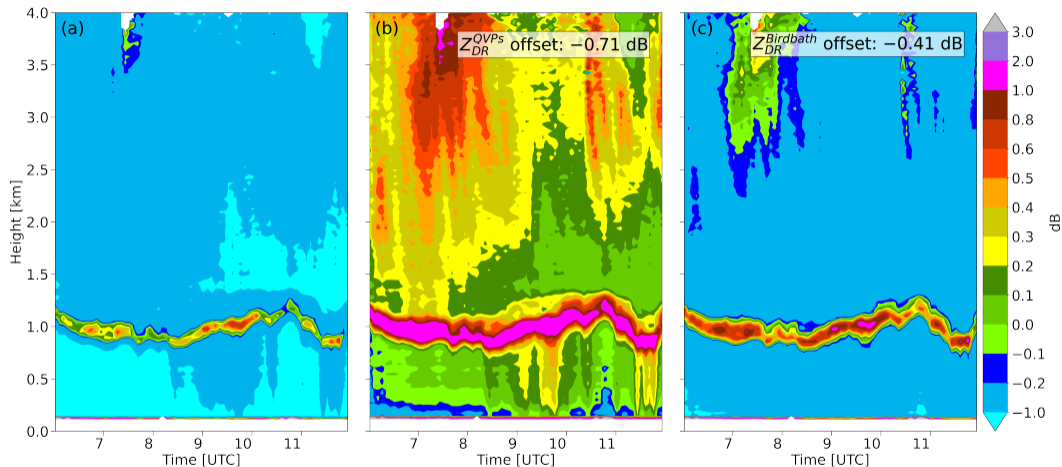


Figure 4: QVPs of Z_{DR} not offset corrected (a), offset corrected using QVP method (b) and birdbath scan method (c) for the 1st January 2013, from 6 UTC to 12 UTC.

Daily Z_{DR} offsets comparison

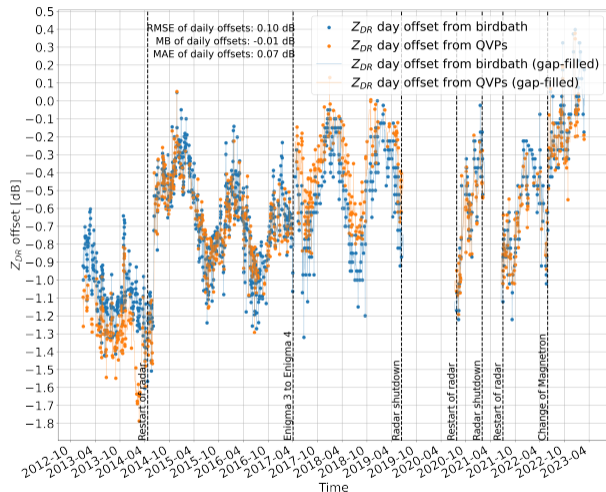


Figure 5: Daily Z_{DR} offsets calculated using QVP (orange) and birdbath scan (blue) method in the period between January 2013 to March 2023. The times of important changes in BoXPoL are given as vertical dashed lines with the respective caption.

Reverse Z_H - Z_{DR} method to correct Z_H

- Calibration of Z_H is performed using Z_H - Z_{DR} relation [Ryzhkov and Zrnice, 2019] but offset corrected Z_{DR} as the predictor
→ highly dependant on an accurate calibration of Z_{DR} .

Reverse Z_H - Z_{DR} method to correct Z_H

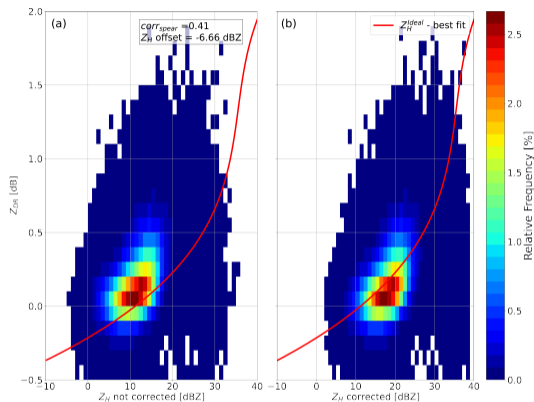


Figure 6: 2D histogram of offset corrected Z_{DR} versus Z_H not offset corrected (a) and offset corrected (b) for the 1 January 2013, using the proposed reverse Z_H - Z_{DR} method. The thick red line indicates the calculated ideal (best fit) Z_H (Z_H^{ideal}).

$$Z_H^{off} = med_{day}[Z_H^{measured} - Z_H^{ideal}]$$

Comparison of Z_H corrected and uncorrected

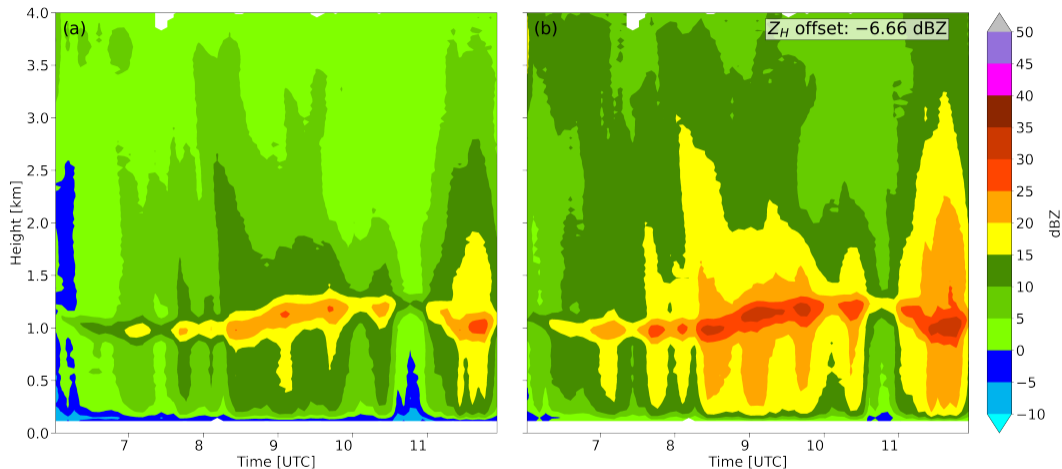


Figure 7: QVPs of (a) uncorrected and (b) corrected Z_H using the reverse Z_H - Z_{DR} method for the 1 January 2013, from 06:00 UTC to 12:00 UTC.

Self consistency relations for Z_H correction

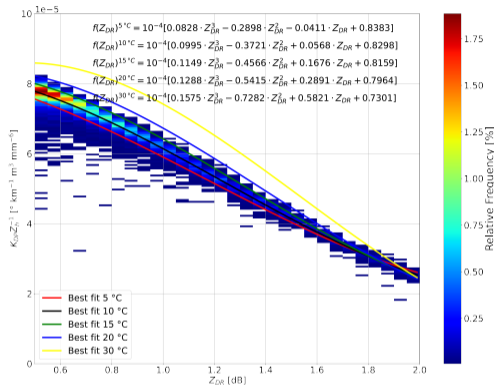


Figure 8: T-matrix simulated $(K_{DP}Z_h^{-1})$ - Z_{DR} dependencies at 18° elevation angle and 10°C based on disdrometer measurements [Chen et al., 2021] with best fit lines using various temperatures.

$$Z_H^{\text{off-selfcon}} = \text{med}_{\text{day}} \left[\text{med}_{\text{height}} \left(10 \log_{10} \left(\frac{f(Z_{DR})Z_h}{K_{DP}} \right) \right) \right]$$

Daily Z_H offset comparison

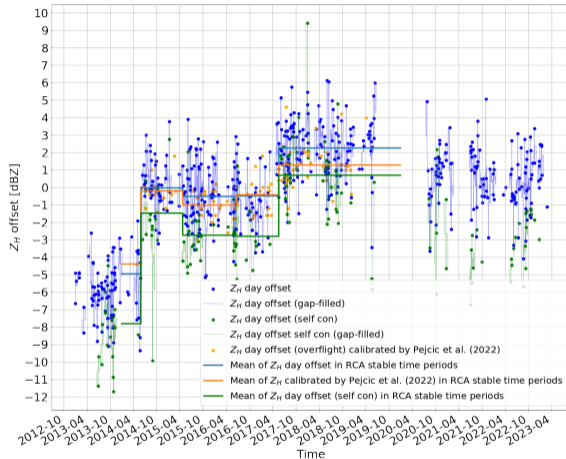


Figure 9: Daily Z_H offsets calculated using the reverse Z_H-Z_{DR} method (blue), the self-consistency method (green) and the daily Z_H offsets obtained by GPM overflights in the period between January 2013 to March 2023 [Pejcic et al., 2022] (orange).

Daily Z_H offset comparison

	Z_H offsets	Z_H offsets in RCA stable periods
RMSE [dBZ]	1.88	0.70
MAE [dBZ]	1.51	0.60
MB [dBZ]	-0.36	-0.50
	Z_H offsets (self con)	Z_H offsets (self con) in RCA stable periods
RMSE [dBZ]	2.28	1.62
MAE [dBZ]	1.91	1.37
MB [dBZ]	1.14	1.37

- Z_{DR} offsets obtained using QVPs in light are reasonable in terms of RMSE and MAE (in the period when the bird bath scanning technique was reliable).
- Mean Z_H offsets obtained agree well with GPM derived mean Z_H offsets in stable RCA time periods between 2014 and 2019.

- Z_{DR} offsets obtained using QVPs in light are reasonable in terms of RMSE and MAE (in the period when the bird bath scanning technique was reliable).
- Mean Z_H offsets obtained agree well with GPM derived mean Z_H offsets in stable RCA time periods between 2014 and 2019.
 - Also the point-to-point comparison shows similar trends and acceptable RMSE and MAE.

- Z_{DR} offsets obtained using QVPs in light are reasonable in terms of RMSE and MAE (in the period when the bird bath scanning technique was reliable).
- Mean Z_H offsets obtained agree well with GPM derived mean Z_H offsets in stable RCA time periods between 2014 and 2019.
 - Also the point-to-point comparison shows similar trends and acceptable RMSE and MAE.
 - Outperforms self consistency method in comparison to GPM overflights.

- Z_{DR} offsets obtained using QVPs in light are reasonable in terms of RMSE and MAE (in the period when the bird bath scanning technique was reliable).
- Mean Z_H offsets obtained agree well with GPM derived mean Z_H offsets in stable RCA time periods between 2014 and 2019.
 - Also the point-to-point comparison shows similar trends and acceptable RMSE and MAE.
 - Outperforms self consistency method in comparison to GPM overflights.



10-Year climatology of vertical profiles (QVPs) of BoXPoI in stratiform conditions

T. Scharbach^{1,2}, S. Trömel¹

¹ Institute for Geosciences, Department Meteorology, University of Bonn, 53121, Germany;

² toscha@uni-bonn.de

Annual Cycles of variables defining/describing the ML

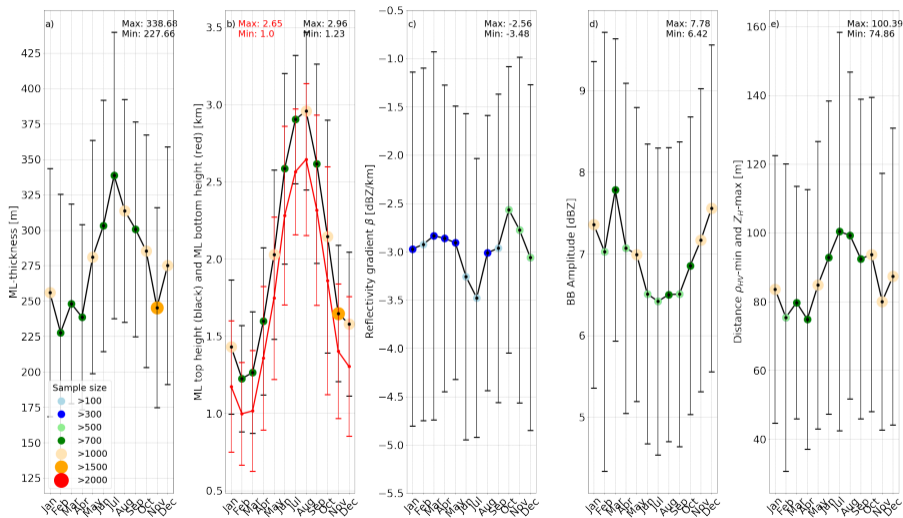


Figure 10: Annual cycles of ML describing variables with sample size per month of the large climatology.

Annual Cycles of variables defining/describing the ML

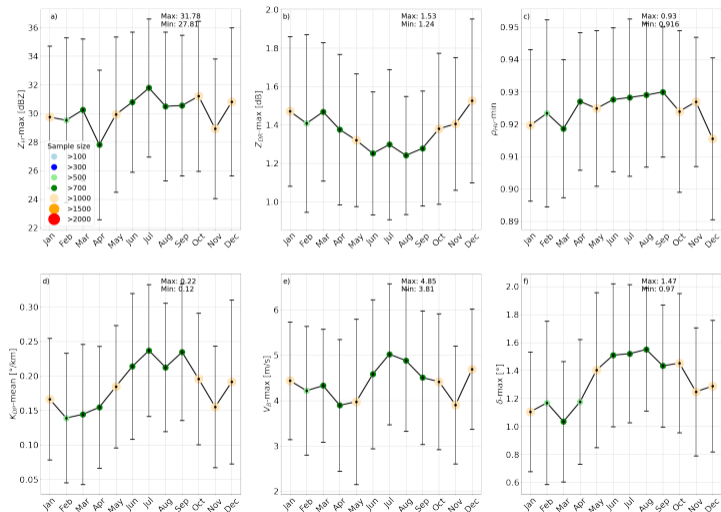


Figure 11: Annual cycles of ML describing variables with sample size per month of the large climatology.

Annual Cycles of variables describing the DGL and region between DGL and ML

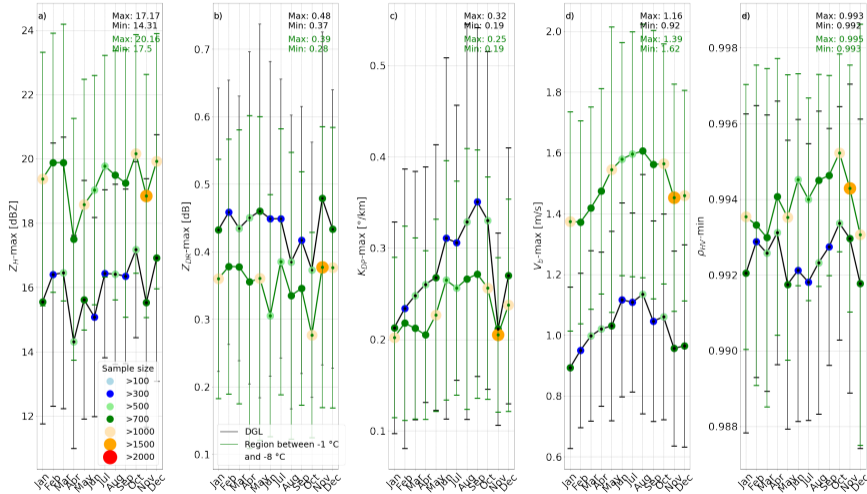


Figure 12: Annual cycles of DGL (black lines) and region between DGL and ML describing variables (green lines) with sample size per month of the large climatology.

Annual Cycles of N_t , D_m and IWC in the DGL and region between DGL and ML

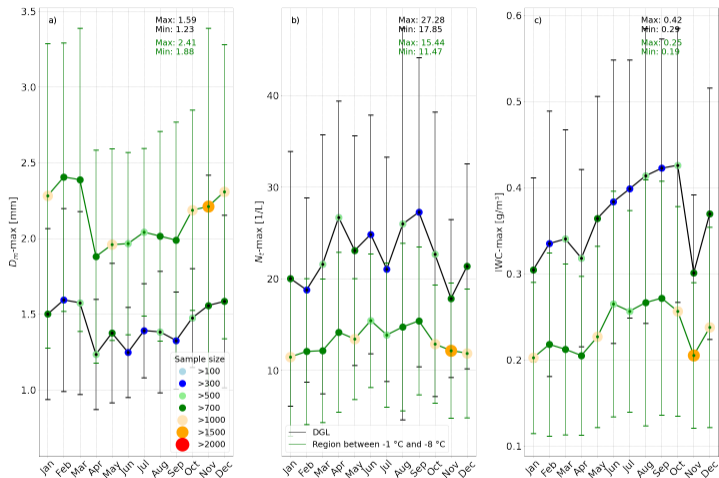


Figure 13: Annual cycles of ice-microphysical retrievals in the DGL and needle growth zone with sample size per month of the large climatology.

Correlation between ML-ML, DGL-DGL and DGL-ML variables

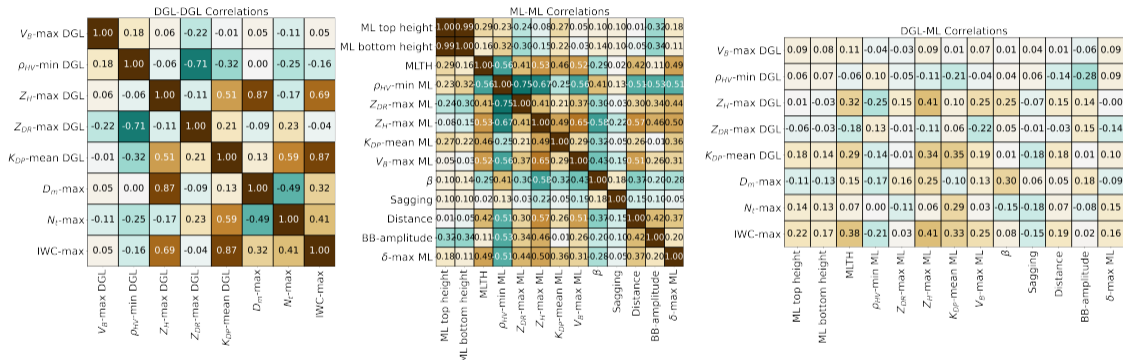


Figure 14: Correlation matrices using spearman correlation coefficient, between ML-ML, DGL-DGL and DGL-ML variables of the full 10 year climatology (Annual cycles are removed before calculation).

Correlation between DGL-Others, Others-Others and Others-ML variables

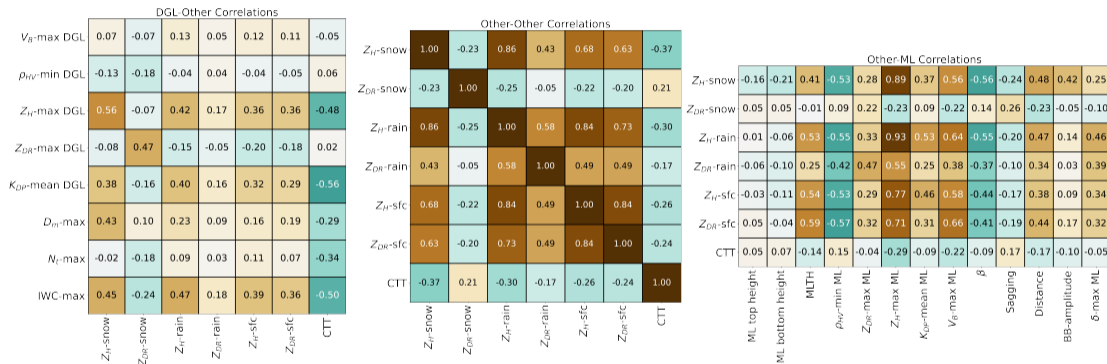





Figure 15: Correlation matrices using spearman correlation coefficient, between DGL-Others, Others-Others and Others-ML variables of the full 10 year climatology (Annual cycles are removed before calculation).

-  Chen, J.-Y., Trömel, S., Ryzhkov, A., and Simmer, C. (2021).
Assessing the benefits of specific attenuation for quantitative precipitation estimation with a c-band radar network.
Journal of Hydrometeorology, 22(10):2617–2631.
-  Pejcic, V., Soderholm, J., Mühlbauer, K., Louf, V., and Trömel, S. (2022).
Five years calibrated observations from the university of bonn x-band weather radar (boxpol).
Scientific Data, 9(1):1–9.
-  Ryzhkov, A. V. and Zrnica, D. S. (2019).
Radar polarimetry for weather observations.
Springer.